I S A V

Journal of Theoretical and Applied Vibration and Acoustics

journal homepage: http://tava.isav.ir

A new analytical approach for axisymmetric free vibration of circular magnetorheological fluid sandwich plate

Seyyed Mahmoud Alavi[a], Mohammad Fadaee[b*], Ali Koochakinejad[c]

[a]*M.Sc., Department of Mechanical Engineering, Qom University of Technology, Qom, Iran*

[b]*Associate Professor, Department of Mechanical Engineering, Qom University of Technology, Qom, Iran*

[c]*M.Sc., Department of Mechanical Engineering, Technical and Vocational University (TVU), Tehran, Iran*

ARTICLE INFO

Article history:

Received 2 November 2019
Received in revised form
8 June 2020

Accepted 1 December 2020

Available online 5 December 2020

Keywords:
Circular sandwich plate,

Magnetorheological fluid,

Axisymmetric vibration,

Exact solution,

Free damped vibration.

ABSTRACT

An exact closed-form solution was introduced to analyze axisymmetric free damped vibration of circular magnetorheological fluid (MRF) sandwich plate. Hamilton principle, as well as the classical thin plate theory were used to extract three fully coupled governing equations of motion and the corresponding boundary conditions. Shear modulus of the MRF was tunable by changing a magnetic field which was perpendicular to the mid-plane of the plate. Using two new functions named as phase and anti-phase in-plane displacement functions (PIDF and AIDF), transverse displacement of the sandwich plate was firstly decoupled and finally, in-plane displacements of the top and bottom layers were extracted to obtain the frequency equation for clamped, simply supported and free boundary conditions. Accuracy and stability of results were assessed according to a finite element analysis. The role of various parameters on variations of natural frequencies and loss factors was investigated. Considering obtained results, it was found that despite the insensitivity of natural frequencies to the intensity of the magnetic field and the MRF thickness variations, the loss factors showed high sensitivity to these parameters. Also, the slope of the plate has a significant role in the dissipated energy of the sandwich circular plate. These findings can be applied by engineers and researchers in designing magnetically controlled devices such as brakes or clutches and heavy motor dampers.

[*] Corresponding author:
E-mail address: fadaee@qut.ac.ir (M. Fadaee)

http://dx.doi.org/10.22064/tava.2021.131640.1172

1. Introduction

Applications of magnetorheological fluids in mechanical structures are increasing dramatically and this justifies the necessity of scientific research on this subject. The MRFs are implemented as controllable layers between elastic layers of structure and can improve the vibration control performance in a wide frequency range [1]. These smart materials supply reversible and rapid changes of damping and stiffness due to the magnetic field intensity.

Due to its special shape, circular sandwich plates have attracted more attention than other plate types in engineering applications, especially in rotating components and where high stiffness to weight ratio is needed. Employing the MRF layer in a sandwich plate for vibration attenuation is a low-cost and reliable method in which some researchers have used them. Eshaghi *et a*l.[2-4] reported experimental and theoretical studies of vibration analysis and optimum design of magnetorheological fluid rectangular and circular sandwich plates. A finite element model and Ritz method were employed to solve the problem using the Kirchhoff plate theory. Ghorbanpour Arani *et al*.[5] analyzed vibration behavior of a magnetorheological rectangular sandwich plate resting on a visco-Pasternak foundation. The sandwich plate consisted of viscoelastic nanocomposite face sheets. The equations of motion were derived by using Hamilton's principle and solved by employing an appropriate analytical method. Arumugam *et al*. [6] studied the dynamic and instability analysis of a rotating composite MRF sandwich plate exposed to a periodic in-plane loading. The equation of motion was derived based on the classical laminated plate theory and provided in the finite element formulation. Hasheminejad and Maleki [7] developed a dynamic model for the vibrational response of a rectangular electrorheological sandwich plate subjected to a general harmonic transverse excitation. Yeh [8] investigated free vibration of rectangular sandwich plates with magnetorheological elastomer core. Modal damper and natural frequencies of the sandwich plate were presented by utilizing the finite element method. Manoharan *et al*. [9] considered the dynamic properties of a laminated composite magnetorheological fluid sandwich plate.The equations of motion were reformulated and solved by using a finite element formulation. Joseph and Mohanty [10, 11] presented the modal and buckling analysis of a skew viscoelastic sandwich plate containing a functionally graded constraining layer. The finite element method, as well as the Mindlin plate theory, was used to solve the plate problem. Ying *et al*. [12] constructed sandwich plates with a magnetorheological core for micro-vibration control. The sandwich plate under stochastic support motion excitation was studied. Yeh [13] analyzed free vibration of rotating polar orthotropic sandwich annular plate with electrorheological fluid core. Hasheminejad *et al*. [14] and Rahiminasab and Rezaeepazhand [15] studied the aeroelastic stability of electrorheological fluid sandwich plates. Amir *et al*. [16] investigated on free vibration of MRF circular plates with magnetostrictive face layers and resting on visco-Pasternak elastic foundation. Soror *et al.* [17] studied vibration analysis of MRF sandwich beams containing an axially functionally graded constraining layer. Ebrahimi and Sedighi [18] presented a study of wave propagation of a rectangular sandwich composite plate with a tunable magnetorheological fluid core. Ghorbanpour Arani and Jamali [19] considered the vibration behavior of a cylindrically curved sandwich plate resting on Winkler–Pasternak substrate.

According to the comprehensive literature survey, despite being many papers in the field of vibration analysis of magnetorheological circular sandwich plate, an exact closed-form solution procedure has been neglected. Hence, this paper presented a new analytical solution to obtain

natural frequencies, corresponding loss factors, and vibrational mode shapes of adaptive circular sandwich plates with the MRFs core. The main difference between the present analytical procedure and those reported by the literature laid in that in this study, the vibration behavior of a circular MRF sandwich plate was analytically investigated using new auxiliary functions as the phase and anti-phase in-plane displacement functions. Finally, the in-plane and out-of-plane displacements of the plate were exactly decoupled. Validation and parametric studies were carried out for various boundary conditions such as clamped, simply supported, and free.

2. Mathematical formulations

2.1. Configuration and constitutive relations

A three-layer solid circular sandwich plate including two top and bottom Aluminum layers and one MRF core layer is showed in Fig. 1. The plate has radius *R* and face layer thicknesses *h*. Also, the core thickness is nominated as *H*. The following assumptions were considered as

1: Slippage between the elastic layers and the core one is negligible.

2: The transverse displacements of the top and bottom layers should be equal.

3: The skins are included in a plane strain contemplate.

4: An axisymmetric motion is supposed for the plate.

Therefore, based on the thin plate theory, the displacement filed of top and bottom layers can be written as [3]

$$u_r^{(j)}(r,z_j,t) = u^{(j)}(r,t) - z_j \frac{\partial w(r,t)}{\partial r} \tag{1a}$$

$$u_\theta^{(j)}(r,z_j,t) = 0 \tag{1b}$$

$$u_z^{(j)}(r,z_j,t) = w(r,t) \tag{1c}$$

where *j=1* and *3* correspond to the top and bottom layers, respectively. *t* is time. The (r,θ,z), (r,θ,z_1) and (r,θ,z_2) are the polar coordinate systems originated at the center of the circular plate resting on the middle surface of the core, top and bottom layers, respectively. $u^{(1)}(r,t)$ and $u^{(3)}(r,t)$ are the axisymmetric in-plane displacements of top, and bottom layers, respectively. $w(r,t)$ is the axisymmetric transverse displacement of the plate.

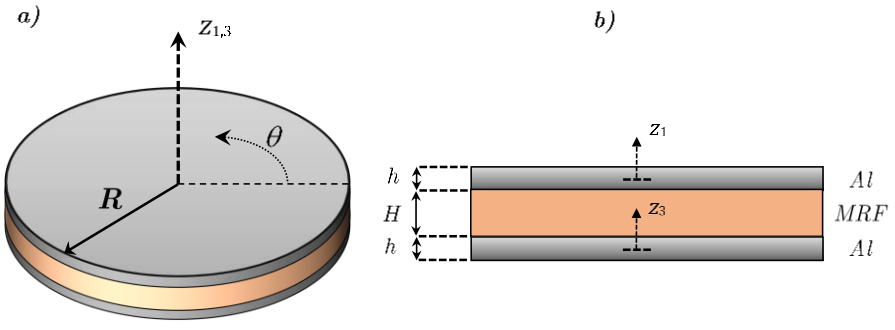

Fig. 1. Configuration of an MR solid circular sandwich plate. a) 3D view b) Cross section.

Due to the aforementioned assumptions, the MRF layer will only be exposed by a shear strain γ_{rz}. Also, normal strains $\varepsilon_{rr}^{(j)}$ and $\varepsilon_{\theta\theta}^{(j)}$ are produced in the elastic layers as [3]

$$\gamma_{rz} = \frac{D}{H}\frac{\partial w}{\partial r} + \frac{u^{(1)} - u^{(3)}}{H} \tag{2a}$$

$$\varepsilon_{rr}^{(j)} = \frac{\partial u_r^{(j)}}{\partial r} \tag{2b}$$

$$\varepsilon_{\theta\theta}^{(j)} = \frac{u_r^{(j)}}{r} \quad , \quad j = 1, \tag{2c}$$

where $D=H+h$.

Based on the Hook's law, we can write as

$$\sigma_{rz} = \tilde{G}\gamma_{rz} \tag{3a}$$

$$\sigma_{rr}^{(j)} = \frac{E}{(1-\nu^2)}\left(\varepsilon_{rr}^{(j)} + \nu\varepsilon_{\theta\theta}^{(j)}\right) \tag{3b}$$

$$\sigma_{\theta\theta}^{(j)} = \frac{E}{(1-\nu^2)}\left(\varepsilon_{\theta\theta}^{(j)} + \nu\varepsilon_{rr}^{(j)}\right) \quad , \quad j = 1,3 \tag{3c}$$

where E and ν are the elasticity modulus and Poisson's ratio of the face layers, respectively. The shear modulus of the MRF core layer $\tilde{G}$ is defined as [3]

$$\tilde{G} = G^* + iG\,, \qquad i = \sqrt{-1} \tag{4}$$

where the loss modulus (G) and the storage modulus (G^*) are determined as [3]

$$G^* = -3.3691B^2 + 4997.5B + 0.873 \times 10^6 \tag{5a}$$

$$G = -0.9B^2 + 812.4B + 0.1855 \times 10^6 \tag{5b}$$

where B is the magnetic field intensity in Gauss.

2.2. The governing equations

Hamilton's principle is employed to obtain the equations of motion and corresponding boundary conditions as

$$\delta \int_0^t (T - U)dt = 0 \tag{6}$$

where δ is the variational operator. T and U are the total kinetic and strain energies as [3]

$$\delta U = \sum_{j=1,3} \int_0^R \int_{-\frac{h}{2}}^{\frac{h}{2}} \left(\sigma_{rr}^{(j)} \delta \varepsilon_{rr}^{(j)} + \sigma_{\theta\theta}^{(j)} \delta \varepsilon_{\theta\theta}^{(j)} \right) r dz_j dr + \int_0^R \int_{-\frac{H}{2}}^{\frac{H}{2}} (\sigma_{rz} \delta \gamma_{rz}) r dz dr \tag{7a}$$

$$\delta T = \sum_{j=1,3} \int_0^R \int_{-\frac{h}{2}}^{\frac{h}{2}} \left(\rho_j (\dot{u}_r^{(j)} \delta \dot{u}_r^{(j)} + \dot{w}^{(j)} \delta \dot{w}^{(j)} \right) r dz_j dr + \int_0^R [(\rho_2 H (\dot{w} \delta \dot{w}) + I_2 (\dot{\gamma}_{rz} \delta \dot{\gamma}_{rz})] r dr \tag{7b}$$

where the dot notation $\dot{(\,)}$ is the first partial derivative with respect to *t*. Substituting Eqs. (7) into (6) as well as using the integration by parts leads to

$$\left(\frac{\partial N_{rr}^{(1)}}{\partial r} r \right) + N_{rr}^{(1)} - N_{\theta\theta}^{(1)} - \frac{Q_{rz}}{H} r = r I_{11} \ddot{u}^{(1)} + r \frac{I_2 D}{H^2} \frac{\partial \ddot{w}}{\partial r} + r I_2 \frac{\ddot{u}^{(1)}}{H^2} - r I_2 \frac{\ddot{u}^{(3)}}{H^2} \tag{8a}$$

$$\left(\frac{\partial N_{rr}^{(3)}}{\partial r} r \right) + N_{rr}^{(3)} - N_{\theta\theta}^{(3)} + \frac{Q_{rz}}{H} r = r I_{31} \ddot{u}^{(3)} - r \frac{I_2 D}{H^2} \frac{\partial \ddot{w}}{\partial r} - r I_2 \frac{\ddot{u}^{(1)}}{H^2} + r I_2 \frac{\ddot{u}^{(3)}}{H^2} \tag{8b}$$

$$\begin{aligned} &\left(\frac{\partial^2 M_{rr}^{(1)}}{\partial r^2} r \right) + 2 \frac{\partial M_{rr}^{(1)}}{\partial r} - \frac{\partial M_{\theta\theta}^{(1)}}{\partial r} + \left(\frac{\partial^2 M_{rr}^{(3)}}{\partial r^2} r \right) + 2 \frac{\partial M_{rr}^{(3)}}{\partial r} - \frac{\partial M_{\theta\theta}^{(1)}}{\partial r} + \left(r \frac{D}{H} \frac{\partial Q_{rz}}{\partial r} \right) \\ &+ \frac{D}{H} Q_{rz} \\ &= -r I_{22} \frac{\partial^2 \ddot{w}}{\partial r^2} + r I_{11} \ddot{w} - I_{33} \frac{\partial \ddot{w}}{\partial r} + r I_{31} \ddot{w} + r I_{21} \ddot{w} - \frac{I_2 D^2}{H^2} \frac{\partial \ddot{w}}{\partial r} \\ &- r \frac{I_2 D^2}{H^2} \frac{\partial^2 \ddot{w}}{\partial r^2} - \frac{I_2 D}{H^2} \ddot{u}^{(1)} + \frac{I_2 D}{H^2} \ddot{u}^{(3)} - I_{22} \frac{\partial \ddot{w}}{\partial r} - r I_{33} \frac{\partial^2 \ddot{w}}{\partial r^2} - r I_2 \frac{D}{H^2} \frac{\partial \ddot{u}^{(1)}}{\partial r} \\ &+ r I_2 \frac{D}{H^2} \frac{\partial \ddot{u}^{(3)}}{\partial r} \end{aligned} \tag{8c}$$

where the double dot notation $\ddot{(\,)}$ is the second partial derivative with respect to *t* and

$$\left(N_{rr}^{(j)}, N_{\theta\theta}^{(j)} \right) = \int_{-\frac{h}{2}}^{\frac{h}{2}} \left(\sigma_{rr}^{(j)}, \sigma_{\theta\theta}^{(j)} \right) dz_j \tag{9a}$$

$$\left(M_{rr}^{(j)}, M_{\theta\theta}^{(j)} \right) = \int_{-\frac{h}{2}}^{\frac{h}{2}} \left(\sigma_{rr}^{(j)} z_j, \sigma_{\theta\theta}^{(j)} z_j \right) dz_j \tag{9b}$$

$$Q_{rz} = \int_{-\frac{H}{2}}^{\frac{H}{2}} \sigma_{rz} dz \tag{9c}$$

$$\begin{aligned} &I_{31} = I_{11} = \int_{-\frac{h}{2}}^{\frac{h}{2}} \rho_j dz_j \quad , \quad I_{22} = I_{33} = \int_{-\frac{h}{2}}^{\frac{h}{2}} \rho_j z_j^2 dz_j \quad , \\ &I_{21} = \int_{-\frac{H}{2}}^{\frac{H}{2}} \rho_2 dz \quad , \quad I_2 = \int_{-\frac{H}{2}}^{\frac{H}{2}} \rho_2 z^2 dz \qquad , \qquad j = 1,3 \end{aligned} \tag{9d}$$

where $\rho_j \ (j = 1,3)$ and ρ_2 are mass density of the face layers and the MRF core layer, respectively. Also, the corresponding boundary conditions of plate's outer edge (i.e. at $r = R$) are derived as

Clamped edge:

$$w = 0\,, u^{(1)} = 0\,, u^{(3)} = 0\,, \frac{\partial w}{\partial r} = 0 \tag{10a}$$

Simply supported edge:

$$N_{rr}^{(1)} = 0\,, N_{rr}^{(3)} = 0\,, w = 0\ \,, M_{rr}^{(1)} + M_{rr}^{(3)} = 0 \tag{10b}$$

Free edge:

$$\begin{aligned} N_{rr}^{(1)} = 0\,, N_{rr}^{(3)} = 0\,, M_{rr}^{(1)} + M_{rr}^{(3)} \\ = 0\ 0, r\frac{\partial M_{rr}^{(1)}}{\partial r} + M_{rr}^{(1)} - M_{\theta\theta}^{(1)} + \ r\frac{\partial M_{rr}^{(3)}}{\partial r} + M_{rr}^{(3)} - M_{\theta\theta}^{(3)} + r\frac{D}{H}Q_{rz} + rI_{22}\frac{\partial \ddot{w}}{\partial r} \\ + rI_{33}\frac{\partial \ddot{w}}{\partial r} + r\frac{I_2 D^2}{H^2}\frac{\partial \ddot{w}}{\partial r} + rI_2\frac{D}{H^2}\ddot{u}^{(1)} - rI_2\frac{D}{H^2}\ddot{u}^{(3)} = 0 \end{aligned} \tag{10c}$$

Where

$$N_{rr}^{(j)} = \left[\left(A\frac{\partial u^{(j)}}{\partial r}\right) + \nu\left(A\frac{u^{(j)}}{r}\right)\right]\ \ ,\ \ N_{\theta\theta}^{(j)} = \left[\left(A\frac{u^{(j)}}{r}\right) + \nu\left(A\frac{\partial u^{(j)}}{\partial r}\right)\right] \tag{11a}$$

$$M_{rr}^{(j)} = \left[\left(-C\frac{\partial^2 w}{\partial r^2}\right) + \nu\left(-C\frac{\partial w}{r\partial r}\right)\right]\ \ ,\ \ M_{\theta\theta}^{(j)} = [\left(-C\frac{\partial w}{r\partial r}\right) + \nu\left(-C\frac{\partial u^{(j)}}{\partial r}\right)] \tag{11b}$$

$$Q_{rz} = [\tilde{G}D\frac{\partial w}{\partial r} + \tilde{G}(u^{(1)} - u^{(3)})] \tag{11c}$$

$$A = \int_{-\frac{h}{2}}^{\frac{h}{2}} \frac{E}{(1-\nu^2)}dz_j\ \ ,\ \ C = \int_{-\frac{h}{2}}^{\frac{h}{2}} \frac{E}{(1-\nu^2)}{z_j}^2 dz_j \tag{11d}$$

Because the geometry and material of the top and bottom layers are similar, *A* and *C* coefficients are equal for both layers. Now, due to assuming a harmonic motion for the plate, we can show the displacement components as [3]

$$u^{(j)}(r,t) = \tilde{u}^{(j)}(r)e^{i\omega t} \tag{12a}$$

$$w(r,t) = \tilde{w}(r)e^{i\omega t} \tag{12b}$$

where ω is the complex natural frequency. Employing of Eqs. (9), (11), and (12) into (8) and doing some simplifications, the equations of motion can be reformulated as

$$A\nabla^2\tilde{u}^{(1)} - A\frac{\tilde{u}^{(1)}}{r^2} + \tilde{u}^{(1)}\left[-\frac{\tilde{G}}{H} + \lambda I_{11} + \frac{\lambda I_2}{H^2}\right] + \tilde{u}^{(3)}\left[\frac{\tilde{G}}{H} - \frac{\lambda I_2}{H^2}\right] + \frac{\partial \tilde{w}}{\partial r}\left[\frac{\lambda I_2 D}{H^2} - \frac{\tilde{G}D}{H}\right] = 0 \tag{13a}$$

$$\begin{aligned} A\nabla^2\tilde{u}^{(3)} - A\frac{\tilde{u}^{(3)}}{r^2} + \tilde{u}^{(3)}\left[-\frac{\tilde{G}}{H} + \lambda I_{11} + \frac{\lambda I_2}{H^2}\right] + \tilde{u}^{(1)}\left[\frac{\tilde{G}}{H} - \frac{\lambda I_2}{H^2}\right] \\ + \frac{\partial \tilde{w}}{\partial r}\left[-\frac{\lambda I_2 D}{H^2} + \frac{\tilde{G}D}{H}\right] = 0 \end{aligned} \tag{13b}$$

$$-2C\nabla^4\widetilde{w}+\frac{D^2\tilde{G}}{H}\nabla^2\widetilde{w}-\frac{I_2D^2\lambda}{H^2}\nabla^2\widetilde{w}-2I_{22}\lambda\nabla^2\widetilde{w}+(2I_{11}\lambda+I_{21}\lambda)\widetilde{w}+\left(\frac{D\tilde{G}}{H}-\frac{I_2D\lambda}{H^2}\right)\left(\frac{\tilde{u}^{(1)}}{r}-\frac{\tilde{u}^{(3)}}{r}\right)+\left(\frac{D\tilde{G}}{H}-\frac{I_2D\lambda}{H^2}\right)\left(\frac{\partial\tilde{u}^{(1)}}{\partial r}-\frac{\partial\tilde{u}^{(3)}}{\partial r}\right)=0 \tag{13c}$$

where $\lambda=\omega^2$. Also, ∇^2 and ∇^4 are the Laplace and bi-Laplace operators.

2.3. The exact solution procedure

Now, we introduce two new functions named as the phase and anti-phase in-plane displacement functions abbreviated as the PIDF and AIDF, respectively, as

$$f=\tilde{u}^{(1)}+\tilde{u}^{(3)} \tag{14a}$$

$$g=\tilde{u}^{(1)}-\tilde{u}^{(3)} \tag{14b}$$

The phase in-plane displacement function *f* represents the sum of in-plane displacements of face layers, whereas the anti-phase in-plane displacement function *g* represents the magnitude of difference between in-plane displacements of face layers. Effects of the in-plane stiffness of sandwich plate on its transverse vibration severely depend on the phase function *f*. In other words, decreasing the values of the *f* function leads to decoupling the Eq. (13c) from Eqs. (13a-b) and consequently, the in-plane ($\tilde{u}^{(1)}$, $\tilde{u}^{(3)}$) and transverse ($\widetilde{w}$) displacements will be solved separately[20]. Also, Eq. (2a) reveals that the shear strain in the MRF core depends on the anti-phase function *g*. Hence, increasing the *g* function leads to increasing the shear strain energy and the total stiffness of the sandwich plate. Based on the reasons mentioned above, it is obvious that two-phase and anti-phase functions (i.e., *f* and *g*) have a crucial role in the vibration behavior of the circular MRF sandwich plate. Therefore, the authors decided to use the PIDF and AIDF in the following closed-form solution.

Substitution of Eqs. (14) into (13) leads to

$$A\nabla^2\left(\frac{f+g}{2}\right)-A\frac{(f+g)}{2r^2}+\left(\frac{f+g}{2}\right)\left[-\frac{\tilde{G}}{H}+\lambda I_{11}+\frac{\lambda I_2}{H^2}\right]+\left(\frac{f-g}{2}\right)\left[\frac{\tilde{G}}{H}-\frac{\lambda I_2}{H^2}\right]+\frac{\partial\widetilde{w}}{\partial r}\left[\frac{\lambda I_2D}{H^2}-\frac{\tilde{G}D}{H}\right]=0 \tag{15a}$$

$$A\nabla^2\left(\frac{f-g}{2}\right)-A\frac{(f-g)}{2r^2}+\left(\frac{f-g}{2}\right)\left[-\frac{\tilde{G}}{H}+\lambda I_{11}+\frac{\lambda I_2}{H^2}\right]+\left(\frac{f+g}{2}\right)\left[\frac{\tilde{G}}{H}-\frac{\lambda I_2}{H^2}\right]+\frac{\partial\widetilde{w}}{\partial r}\left[-\frac{\lambda I_2D}{H^2}+\frac{\tilde{G}D}{H}\right]=0 \tag{15b}$$

$$-2C\nabla^4\widetilde{w}+\frac{D^2\tilde{G}}{H}\nabla^2\widetilde{w}-\frac{I_2D^2\lambda}{H^2}\nabla^2\widetilde{w}-2I_{22}\lambda\nabla^2\widetilde{w}+(2I_{11}\lambda+I_{21}\lambda)\widetilde{w}+\left(\frac{D\tilde{G}}{H}-\frac{I_2D\lambda}{H^2}\right)\left(\frac{g}{r}\right)+\left(\frac{D\tilde{G}}{H}-\frac{I_2D\lambda}{H^2}\right)\left(\frac{\partial g}{\partial r}\right)=0 \tag{15c}$$

Now, summing and subtracting Eqs. (15a) and (15b) give respectively as

$$A\nabla^2 f - \frac{A}{r^2} f + \lambda I_{11} f = 0 \tag{16a}$$

$$A\nabla^2 g - \frac{A}{r^2} g + 2\left(\frac{\lambda I_2 D}{H^2} - \frac{\tilde{G} D}{H}\right)\frac{\partial \widetilde{w}}{\partial r} + \left(2\frac{\lambda I_2}{H^2} - 2\frac{\tilde{G}}{H} + \lambda I_{11}\right) g = 0 \tag{16b}$$

Introducing a new function as

$$p = \frac{\partial g}{\partial r} + \frac{g}{r} \tag{17}$$

we can reformulate Eq. (16b) and Eq. (15c) as

$$\frac{\partial (Eq.(16b))}{\partial r} + \frac{(Eq.(16b))}{r}$$

$$A\nabla^2 p + 2\left(\frac{\lambda I_2 D}{H^2} - \frac{\tilde{G} D}{H}\right)\nabla^2 \widetilde{w} + \left(2\frac{\lambda I_2}{H^2} - 2\frac{\tilde{G}}{H} + \lambda I_{11}\right) p = 0 \tag{18a}$$

$Eq.(15c)$:

$$-2C\nabla^4 \widetilde{w} + \left(\frac{D^2 \tilde{G}}{H} - \frac{I_2 D^2 \lambda}{H^2} - 2I_{22}\lambda\right)\nabla^2 \widetilde{w} + (2I_{11}\lambda + I_{21}\lambda)\widetilde{w} + \left(\frac{D\tilde{G}}{H} - \frac{I_2 D\lambda}{H^2}\right) p = 0 \tag{18b}$$

From Eqs. (18a-b), an explicit expression for the transverse displacement $\widetilde{w}$ can be derived as

$$\nabla^6 \widetilde{w} + a_1 \nabla^4 \widetilde{w} + a_2 \nabla^2 \widetilde{w} + a_3 \widetilde{w} = 0 \tag{19}$$

Where

$$a_1 = \left\{\frac{1}{2C}\left[\frac{-D^2 \tilde{G}}{H} + \lambda\left[\frac{I_2 D^2}{H^2} + 2I_{22}\right]\right] + \frac{1}{A}\left[-\frac{2\tilde{G}}{H} + \lambda\left[\frac{2I_2}{H^2} + I_{11}\right]\right]\right\} \tag{20a}$$

$$a_2 = \left\{\frac{\lambda}{2C}[-2I_{11} - I_{21}] + \frac{\frac{D\tilde{G}}{H} - \frac{I_2 D\lambda}{H^2}}{AC}\left[\frac{\lambda I_2 D}{H^2} - \frac{\tilde{G} D}{H}\right] + \frac{1}{2AC}\left[-\frac{D^2 \tilde{G}}{H}\left[\lambda\left[\frac{2I_2}{H^2} + I_{11}\right] - \frac{2\tilde{G}}{H}\right]\right.\right.$$
$$\left.\left. + \frac{I_2 D^2 \lambda}{H^2}\left[\lambda\left[\frac{2I_2}{H^2} + I_{11}\right] - \frac{2\tilde{G}}{H}\right] + 2I_{22}\lambda\left[-\frac{2\tilde{G}}{H} + \lambda\left[\frac{2I_2}{H^2} + I_{11}\right]\right]\right]\right\} \tag{20b}$$

$$a_3 = \left\{\frac{1}{2AC}\left[-2I_{11}\lambda\left[\lambda\left[\frac{2I_2}{H^2} + I_{11}\right] - \frac{2\tilde{G}}{H}\right] - I_{21}\lambda\left[-\frac{2\tilde{G}}{H} + \lambda\left[\frac{2I_2}{H^2} + I_{11}\right]\right]\right]\right. \tag{20c}$$

The solution of Eqs. (19) may be expressed as [20]

$$\widetilde{w} = \widetilde{w}_1 + \widetilde{w}_2 + \widetilde{w}_3 \tag{21}$$

Where

$$\widetilde{w}_1 = c_1 I_0\left(\sqrt{\alpha_1} r\right) \tag{22a}$$

$$\widetilde{w}_2 = c_2 I_0\left(\sqrt{\alpha_2} r\right) \tag{22b}$$

$$\widetilde{w}_3 = c_3 I_0\left(\sqrt{\alpha_3} r\right) \tag{22c}$$

where $c_1,\ c_2,\ c_3$ are the constant coefficients, I_0 is the zero-order of the first type of modified Bessel function and $\alpha_1, \alpha_2, \alpha_3$ are the roots of the equation as

$$s^3 + a_1 s^2 + a_2 s + a_3 = 0 \tag{23}$$

Also, in order to obtain the PIDF and AIDF functions as the f and g, Eq.(16a) and (17)should be solved as

$$f = c_4 J_1\left(\sqrt{\frac{\lambda I_{11}}{A}} r\right) \tag{24a}$$

$$g = \frac{1}{r}\int_0^r rpdr \tag{24b}$$

where J_1 is the first order of the first type of Bessel function. Also, the c_i $(i = 1 - 4)$ is the mode shape coefficient showing the various shapes of plate vibration modes. Values of these coefficients can be determined by solving the forced vibration problem.

Finally, using Eqs. (24) into (14), the in-plane displacements of the elastic layers can be presented as

$$\tilde{u}^{(1)} = \frac{f + g}{2} \tag{25a}$$

$$\tilde{u}^{(3)} = \frac{f - g}{2} \tag{25b}$$

By applying an arbitrary boundary condition at the outer edge of the plate, the following homogenous linear algebraic equations is found as

$$\begin{aligned} &\mathrm{M}_{4\times4}.C_{4\times1} = 0 \\ &C_{4\times1} = \{c_1, c_2, c_3, c_4\}^T \end{aligned} \tag{26}$$

where **M** is the coefficients matrix and a function of λ^2 only. To obtain a nontrivial solution for Eq. (26), the determinant of **M** must be equal to zero. Therefore, the roots of this equation will be

λ^2. The natural frequencies ω_n and corresponding loss factors η_n can be subsequently extracted by the complex eigenvalue $\lambda = Re(\lambda) + i\, Im(\lambda), i = \sqrt{-1}$ as [3]

$$\omega_n = \sqrt{Re(\lambda^2)} \quad , \qquad \eta_n = \frac{Im(\lambda^2)}{Re(\lambda^2)} \tag{27}$$

3. Results and discussion

First, in order to assess the validity and accuracy of the present approach, we compared the first, second, and third axisymmetric vibration modes of a sandwich solid circular plate with a finite element analysis carried out in ABAQUS software. A circular plate with three layers was modelled in the software. The top and bottom layers were composed of aluminum having the material properties as $\nu = 0.3, \rho = 2700\ kg\ /\ m^3, E = 70\ GPa$ and a core layer was composed of MRF-122EG with $\nu = 0.3$, $\rho = 2300\ {}^{kg}/_{m^3}, E = 2.2698\ MPa$. Three types of edge boundary conditions as simply supported, clamped, and free were imposed to the plate's outer edge. In the software, no tension and linear elastic behavior assumptions were supposed for the MRF core layer. The 3D stress element was employed. In Table 1, the magnetic flux density was zero and $h = 2\ mm, R = 0.1m$. The results showed very good closeness between the present method and the finite element approach. The error percentages between the present results and FEM ones were less than 4%. These error percentages were calculated as

$$Error\ (\%) = \frac{FEM - Present}{FEM} \times 100 \tag{28}$$

Also, a comparison study was performed between the present results and those of Eshaghi *et al.* [3] in Table 2. Results reported by the reference [3] were calculated by experimental and numerical approaches. The following material and geometry parameters were considered for this case: $R = 50\ mm, H = h = 0.5\ mm, \nu = 0.35$, $\rho_1 = \rho_3 = 1600\ kg/m^3, E = 2.2\ GPa$, $\rho_2 = 2500\ kg/m^3$ and $G^*, G = (a_0 + a_1 B + a_2 B^2)(1 - e^{-a_3 \omega})$ where a_i $(i = 0,1,2,3)$ are constants as $a_0 = 97905.69, a_1 = 6744.595, a_2 = 92.75970, a_3 = 0.007328$ for the storage modulus G^* and $a_0 = 41281.45$, $a_1 = 1807.337, a_2 = 8.470100, a_3 = 0.006500$ for the loss modulus G. The boundary condition of plate's outer edge was free. The results revealed that the present results were very close to those of Eshaghi *et al*. [3]. Therefore, the reliability of the approach was validated. The error percentages presented in Table 2 were calculated as

$$\begin{aligned} \text{Error 1 (\%)} &= \frac{\text{Experiment [3]} - \text{Present}}{\text{Experiment [3]}} \times 100 \\ \text{Error 2 (\%)} &= \frac{\text{Ritz [3]} - \text{Present}}{\text{Ritz [3]}} \times 100 \end{aligned} \tag{29}$$

In Figs. 2, 3, and 4, the top and bottom layers were composed of aluminum having the material properties as $\nu = 0.3, \rho = 2700\ kg\ /\ m^3, E = 70\ GPa$ and the MRF layer was composed of MRF-122EG with the material properties mentioned in Eqs. (5). Figs. 2 reports the fundamental natural frequency (Hz) and corresponding loss factor versus the plate radius R(m) when $\mathrm{H} = 1.5\,\mathrm{mm}$, $\mathrm{h} = 2\,\mathrm{mm}$ and $\mathrm{B} = 20\,\mathrm{mT}$. It is noticeable that the natural frequencies and the loss factors are defined as the ratio of total strain energy to the total kinetic energy and the ratio of

energy dissipated per radian to the total strain energy, respectively. The results of Fig. 2 show that when the radius of plate *R* increases, the structural stiffness decreases, leading to a decrease in the total strain energy. Hence, according to the aforementioned definitions of the natural frequencies and loss factors, the fundamental natural frequency decreased and the corresponding loss factor increased. Also, Fig. 2b reveals that the loss factors suddenly decrease when the edge boundary condition changes from the simply supported to the clamped. This shows that according to Eq. (2a), the slope of the plate $\frac{\partial w}{\partial r}$ has a significant role in the dissipated energy of the sandwich circular plate.

Table 1. The first three natural frequencies $\omega_n\ (Hz)$ of MRF sandwich solid circular plate when $h = 2\ mm, R = 0.1m, B = 0$.

Boundary condition	H (mm)	First mode			Second mode			Third mode		
		FEM	Present	*Error (%)*	FEM	Present	*Error (%)*	FEM	Present	*Error (%)*
Clamped	1	467.85	466.37	*0.32*	1786.6	1783.9	*0.15*	3961.8	3977.2	*-0.39*
	1.5	447.58	446.11	*0.33*	1709.7	1709.2	*0.03*	3772.5	3809.9	*-0.99*
	2	430.32	428.90	*0.33*	1641.3	1643.7	*-0.15*	3589.1	3662.9	*-2.06*
Simply supported	1	238.49	239.06	*-0.24*	1338.0	1340.1	*-0.16*	3297.3	3314.3	*-0.52*
	1.5	227.21	227.49	*-0.12*	1280.6	1283.2	*-0.20*	3146.3	3174.6	*-0.90*
	2	218.31	218.48	*-0.08*	1230.4	1233.7	*-0.27*	3004.6	3053.3	*-1.62*
Free	1	433.56	434.71	*-0.27*	1732.2	1667.9	*3.71*	3896.8	3920.9	*-0.62*
	1.5	413.11	413.76	*-0.16*	1656.9	1661.5	*-0.28*	3711.1	3756.1	*-1.21*
	2	396.92	397.46	*-0.14*	1590.7	1596.8	*-0.38*	3532.4	3609.4	*-2.18*

Fig. 3 depicts the fundamental natural frequency (Hz) and loss factor values when the MRF thickness *H*(mm) changes from 0.5 mm to 5 mm. According to Fig. 3(a), by increasing *H*, the kinetic energy of the structure in comparison with its strain energy increased more, leading to a decrease in the natural frequency. Also, Fig. 3(b) shows that when H increases from 0.5 mm to 2 mm (nearly equals to the skin thickness), the loss factor decreases due to increasing the total strain energy. But for H values greater than 2 mm, the loss factor increases monotonically. This is because the increase in the dissipated energy is greater than the increase in the total strain energy. It is worth mentioning that the natural frequency is not very sensitive to change of H, whereas the corresponding loss factor is influenced more.

Table 2. Comparison of first axisymmetric natural frequency Hz of MRF sandwich circular plate.

B (mT)	Method				
	Experiment [3]	Ritz [3]	Present	*Error 1 (%)*	*Error 2 (%)*
0	127.20	118.26	117.11	*7.93*	*0.97*
10	140.60	137.35	135.24	*3.81*	*1.54*
20	152.40	155.90	150.87	*1.00*	*3.23*
30	167.80	172.48	161.54	*3.73*	*6.34*

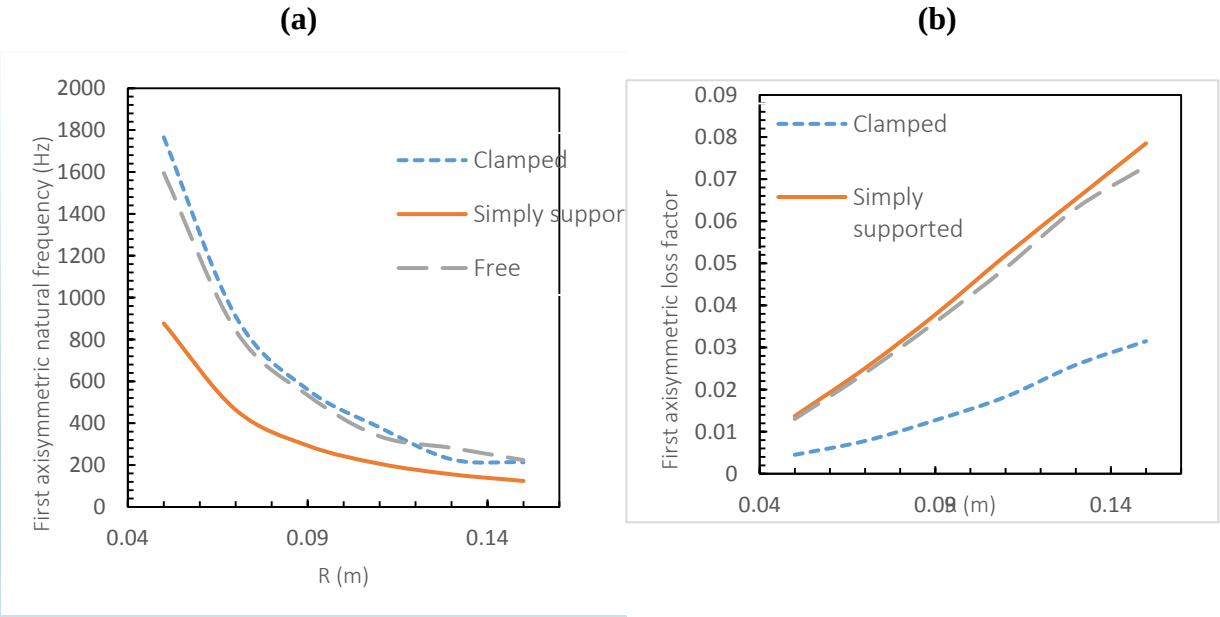

Fig. 2. The fundamental natural frequency (Hz) and loss factor versus the plate radius R(m) for the MR sandwich solid circular plate when $H=1.5\,mm$, $h=2\,mm$ and $B=20\,mT$.

Fig. 4 presents the fundamental natural frequency (Hz) and loss factor changes with respect to the magnetic field intensity B (mT). Regardless of boundary conditions, the fundamental natural frequency and corresponding loss factor initially increase and then decrease slightly when the B is increased. This is due to the direct dependency of the fundamental natural frequency and loss factor to the storage modulus G^* and the loss modulus G, respectively. So that similar to the storage modulus G^* and the loss modulus G, the fundamental natural frequency and loss factor also change according to a quadratic function of the B (see Eq. (5)) with the maximum values at about B=74 mT and B=45 mT, respectively.

Finally, in order to create better insight and understanding about the axisymmetric mode shapes for researchers and engineers who will read this paper, Fig. 5 is provided to present the first three axisymmetric mode shapes of the sandwich plates considered in Table 1.

(a)

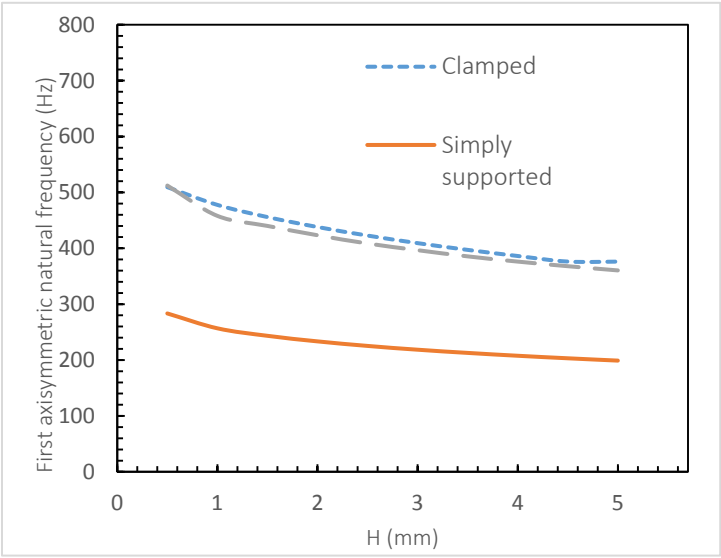

(b)

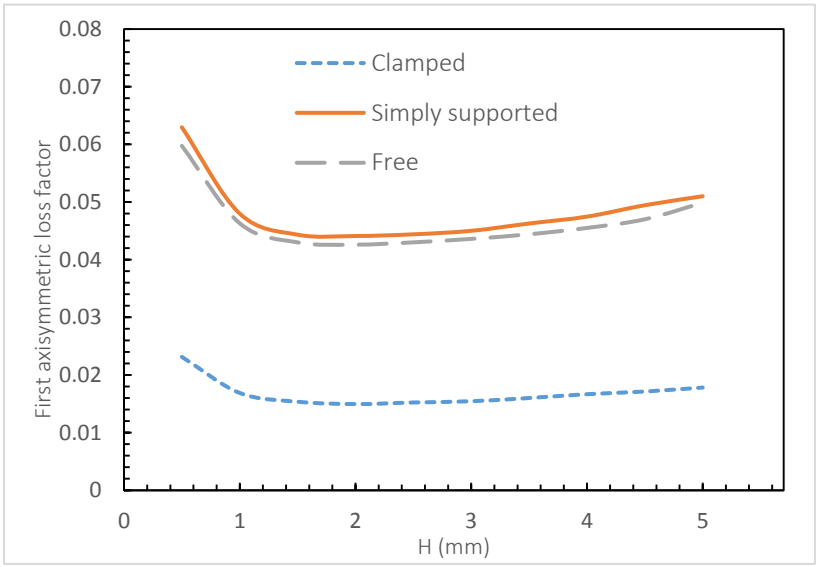

Fig. 3. The fundamental natural frequency (Hz) and loss factor versus the MRF thickness H(mm) for the MR sandwich solid circular plate when $\mathrm{R}=0.1\mathrm{m}$, $\mathrm{h}=2\mathrm{mm}$ and $\mathrm{B}=20\mathrm{mT}$.

(a)

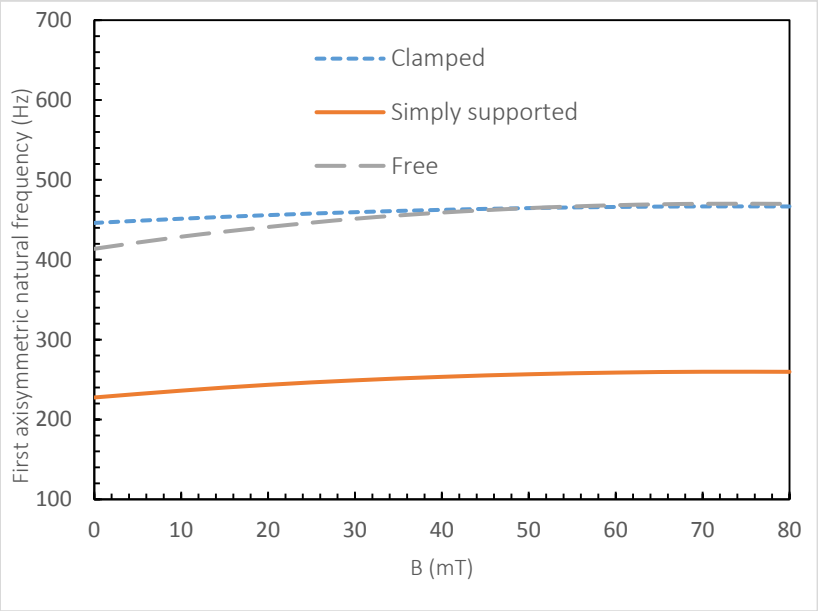

(b)

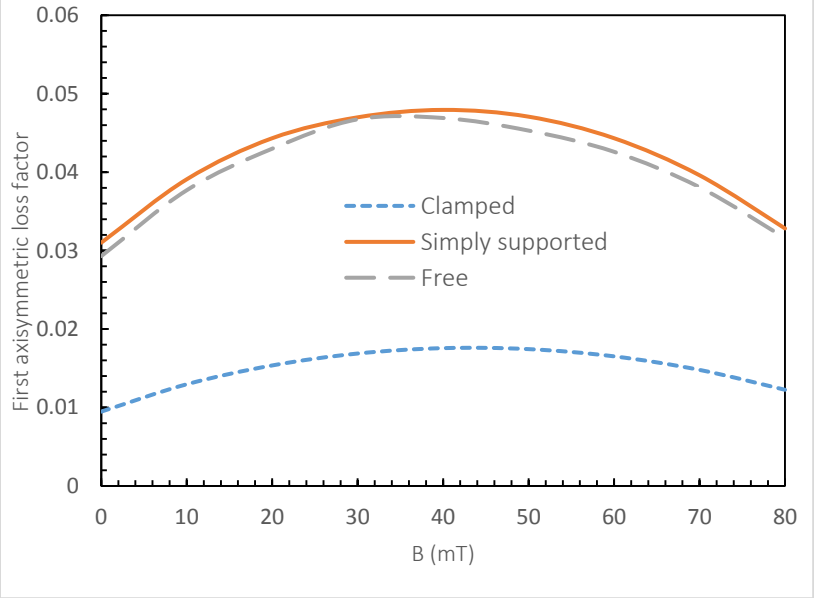

Fig. 4. The fundamental natural frequency (Hz) and loss factor versus the magnetic field intensity B(mT) for the MR sandwich solid circular plate when $R = 0.1\mathrm{m}$, $h = 2\mathrm{mm}$ and $H = 1.5\mathrm{mm}$.

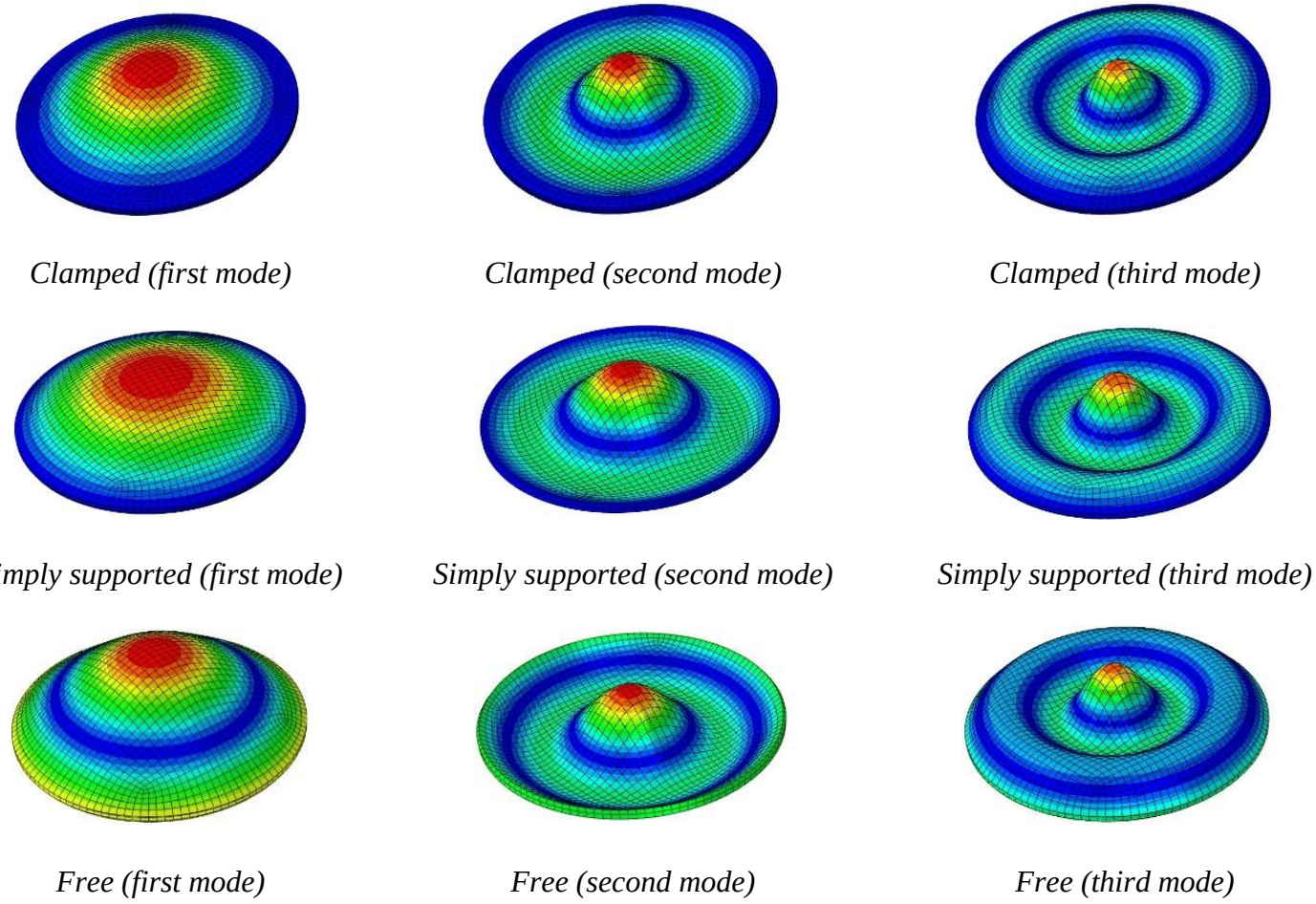

Fig. 5. 3D view of first three mode shapes of an MRF sandwich solid circular plate

4. Conclusion

The scope of this research was to obtain a fully-analytical approach for axisymmetric free vibration of the MRF sandwich circular plates based on the thin sandwich plate theory. By introducing two-phase and anti-phase in-plane displacement functions as well as using some mathematical operations in the polar coordinate, the transverse displacement of the plate was initially extracted. Then, the in-plane displacements of the face elastic layers were analytically derived so as to extract the frequency equation employing the Bessel functions. The validation results reported a high accuracy for the present exact closed-form solution. The results of figures 2, 3, and 4 show that the natural frequencies and corresponding loss factors are strongly influenced by the clamped boundary condition. This happens because the shear strain in the MRF layer is significantly affected by the slope of the plate (see equation 2a). Variations of the MRF layer thickness and the magnetic field intensity affect the loss factor more than the natural frequency. Nevertheless, the radius of the plate causes a significant change in both the natural frequency and corresponding loss factor.

References

[1] R. Ahamed, S.-B. Choi, M.d.M. Ferdaus, A state of art on magneto-rheological materials and their potential applications, Journal of Intelligent Material Systems and Structures, 29 (2018) 2051-2095.
[2] M. Eshaghi, R. Sedaghati, S. Rakheja, The effect of magneto-rheological fluid on vibration suppression capability of adaptive sandwich plates: Experimental and finite element analysis, Journal of Intelligent Material Systems and Structures, 26 (2015) 1920-1935.
[3] M. Eshaghi, R. Sedaghati, S. Rakheja, Analytical and experimental free vibration analysis of multi-layer MR-fluid circular plates under varying magnetic flux, Composite Structures, 157 (2016) 78-86.
[4] M. Eshaghi, R. Sedaghati, S. Rakheja, Vibration analysis and optimal design of multi-layer plates partially treated with the MR fluid, Mechanical Systems and Signal Processing, 82 (2017) 80-102.
[5] A. Ghorbanpour Arani, H. BabaAkbar Zarei, E. Haghparast, Vibration response of viscoelastic sandwich plate with magnetorheological fluid core and functionally graded-piezoelectric nanocomposite face sheets, Journal of Vibration and Control, 24 (2018) 5169-5185.
[6] A.B. Arumugam, M. Ramamoorthy, V. Rajamohan, Dynamic characterization and parametric instability analysis of rotating magnetorheological fluid composite sandwich plate subjected to periodic in-plane loading, Journal of Sandwich Structures & Materials, 21 (2019) 2099-2126.
[7] S.M. Hasheminejad, M. Maleki, Free vibration and forced harmonic response of an electrorheological fluid-filled sandwich plate, Smart Materials and Structures, 18 (2009) 055013.
[8] J.-Y. Yeh, Vibration analysis of sandwich rectangular plates with magnetorheological elastomer damping treatment, Smart Materials and Structures, 22 (2013) 035010.
[9] R. Manoharan, R. Vasudevan, A.K. Jeevanantham, Dynamic characterization of a laminated composite magnetorheological fluid sandwich plate, Smart Materials and Structures, 23 (2014) 025022.
[10] S.V. Joseph, S.C. Mohanty, Buckling and free vibration analysis of skew sandwich plates with viscoelastic core and functionally graded material constraining layer, Proceedings of the Institution of Mechanical Engineers, Part G: Journal of Aerospace Engineering, 233 (2019) 369-381.
[11] S.V. Joseph, S.C. Mohanty, Temperature effects on buckling and vibration characteristics of sandwich plate with viscoelastic core and functionally graded material constraining layer, Journal of Sandwich Structures & Materials, 21 (2019) 1557-1577.
[12] Z.G. Ying, Y.Q. Ni, S.Q. Ye, Stochastic micro-vibration suppression of a sandwich plate using a magneto-rheological visco-elastomer core, Smart materials and structures, 23 (2013) 025019.
[13] J.-Y. Yeh, Free vibration analysis of rotating polar orthotropic annular plate with ER damping treatment, Composites Part B: Engineering, 42 (2011) 781-788.
[14] S.M. Hasheminejad, M. Nezami, M.E.A. Panah, Flutter suppression of an elastically supported plate with electro-rheological fluid core under yawed supersonic flows, International Journal of Structural Stability and Dynamics, 13 (2013) 1250073.
[15] J. Rahiminasab, J. Rezaeepazhand, Aeroelastic stability of smart sandwich plates with electrorheological fluid core and orthotropic faces, Journal of Intelligent Material Systems and Structures, 24 (2013) 669-677.
[16] S. Amir, E. Arshid, Z. Khoddami Maraghi, A. Loghman, A. Ghorbanpour Arani, Vibration analysis of magnetorheological fluid circular sandwich plates with magnetostrictive facesheets exposed to monotonic magnetic field located on visco-Pasternak substrate, Journal of Vibration and Control, 26 (2020) 1523-1537.
[17] A.O. Soroor, M. Asgari, H. Haddadpour, Effect of axially graded constraining layer on the free vibration properties of three layered sandwich beams with magnetorheological fluid core, Composite Structures, 255 (2021) 112899.
[18] F. Ebrahimi, S.B. Sedighi, Wave propagation analysis of a rectangular sandwich composite plate with tunable magneto-rheological fluid core, Journal of Vibration and Control, 27 (2021) 1231-1239.
[19] A. Ghorbanpour Arani, S.A. Jamali, The vibration of the cylindrically curved sandwich plate with rheological core and nanocomposite face sheets rested on the Winkler–Pasternak foundation, Journal of Sandwich Structures & Materials, (2020) 1099636220909818.
[20] S.h. Hosseini-Hashemi, M. Fadaee, M. Es' Haghi, A novel approach for in-plane/out-of-plane frequency analysis of functionally graded circular/annular plates, International Journal of Mechanical Sciences, 52 (2010) 1025-1035.